JACS
JOURNAL OF THE AMERICAN CHEMICAL SOCIETY
Article
pubs.acs.org/JACS

High-Temperature and Pressure-Induced Ferroelectricity in Hydrogen-Bonded Supramolecular Crystals of Anilic Acids and 2,3-Di(2-pyridinyl)pyrazine

Sachio Horiuchi,*[,†,‡] Reiji Kumai,[‡,§] and Yoshinori Tokura[†,∥,⊥]

[†]National Institute of Advanced Industrial Science and Technology (AIST), Tsukuba 305-8562, Japan

[‡]CREST, Japan Science and Technology Agency (JST), Tokyo 102-0076, Japan

[§]Condensed Matter Research Center (CMRC) and Photon Factory, Institute of Materials Structure Science, High Energy Accelerator Research Organization (KEK), Tsukuba 305-0801, Japan

[∥]Department of Applied Physics, The University of Tokyo, Tokyo 113-8656, Japan

[⊥]Correlated Electron Research Group (CERG) and Cross-correlated Materials Research Group (CMRG), RIKEN Advanced Science Institute, Wako 351-0198, Japan

Supporting Information

ABSTRACT: Cocrystallization of anilic acids (H_2xa) and 2,3-di(2-pyridinyl)pyrazine (dppz) affords a variety of molecular geometries, including hydrogen-bonding and supramolecular structures. Proton-transferred 1:1 salts of [H-dppz][Hca] and [H-dppz][Hba] (H_2ca = chloranilic acid, H_2ba = bromanilic acid) were found to host room-temperature ferroelectricity with a spontaneous polarization of 3−4 μC/cm^2 along the hydrogen-bonded chains. Compared with the Curie points of other supramolecular ferroelectrics, those of the salts are relatively high (402 K and >420 K, respectively) because of the elongated hydrogen bonds, which stabilize the proton-ordered state against thermal agitation. In addition to the ferroelectric black (α) form, dppz and H_2ba gave two different crystal forms with a 2:3 ratio: the brown β form of $[H_{1.5}\text{-dppz}]_2[\text{Hba}]_3$ and the brownish-red γ form of $[\text{H-dppz}]_2[\text{Hba}]_2[H_2\text{ba}]$. Mixed solutions of dppz with the less acidic fluoranilic acid (H_2fa) exhibit valence instability; the H_2fa molecules remain mostly neutral in absolute ethanol, whereas methanol (MeOH) solution apparently increases the deprotonated Hfa$^-$ content. Crystallizations of these solutions gave a neutral [dppz][H_2fa] cocrystal and ionic [H-dppz$^+$][Hfa$^-$]·MeOH salt, respectively. The ferroelectricity induced by a modest hydrostatic pressure corroborates the conclusion that the ionic state with a dipolar [H-dppz$^+$][Hfa$^-$] chain is energetically close to the nonpolar neutral ground state of the [dppz][H_2fa] crystal.

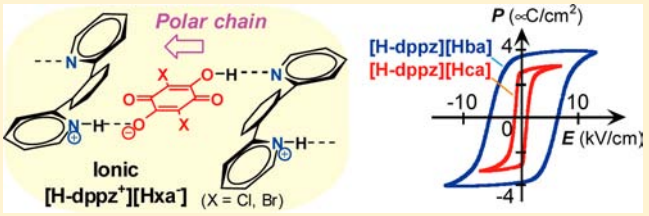

1. INTRODUCTION

The hydrogen-bonding interaction is highly directional and much stronger than the van der Waals interaction, which usually favors close molecular packing. Hydrogen-bond formation is thus often accompanied by some structural flexibility toward the intermolecular space, which can trigger structural phase transitions in various ways.[1] The ferroelectric phase transition to a polar structure with bistable polarities has been one of the most attractive issues because ferroelectrics can accumulate and store large electronic charges by spontaneous polarization, sense temperature changes and mechanical stress, interchange electrical and mechanical energy, modulate light, and transform optical wavelengths.[2] Hydrogen-bonded ferroelectrics of the KH_2PO_4 (KDP) family[3] are representative materials that have been extensively studied to understand the gigantic isotope effect and the role of proton dynamics.[2]

For organic molecular systems, high-performance ferroelectricity is desired for current and future organic electronics and optoelectronics.[4] However, there were only a few examples[5] of such systems until the recent discovery of several supramolecular ferroelectrics of 2,5-dihalo-3,6-dihydroxy-*p*-benzoquinones[6] (haloanilic acid, hereafter designated as H_2xa; Figure 1). Research began with extended chains of alternating proton donors and acceptors, and the hydrogen-bonded neutral cocrystal of phenazine (Phz) with chloranilic acid (H_2ca) or bromanilic acid (H_2ba) exhibited a spontaneous polarization of 1−2 μC cm^{-2} and a large dielectric permittivity of up to 2000−3000.[7] Later, we achieved a higher polarization of 3−4 μC cm^{-2} with a proton-transferred salt derived from 5,5′-dimethyl-2,2′-bipyridine (55dmbp) and iodanilic acid (H_2ia): [H-55dmbp][Hia].[8] The Curie points of these supramolecules were improved to beyond room temperature by deuteration. With the base 2,3,5,6-tetra(2-pyridinyl)pyrazine (tppz), we found 1:2 salts of $[H_2\text{-tppz}][\text{Hxa}]_2$ with distinct supramolecular architectures in which the ferroelectricity is driven by a double-

Received: January 10, 2013
Published: February 28, 2013

   dx.doi.org/10.1021/ja400318v | J. Am. Chem. Soc. 2013, 135, 4492−4500

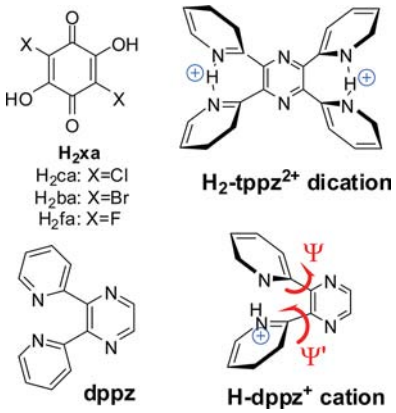

Figure 1. Chemical structures of the anilic acids (H_2xa) and bases. Protonated dppz and tppz can behave as proton sponges, as exemplified by H_2-tppz^{2+}, or adopt various twisted conformations by changing the dihedral angles (Ψ and Ψ′) between the pyrazyl and pyridyl rings.

proton transfer process on the O—H···O-bonded cyclic dimer $[Hxa^-]_2$ and the acentric proton locations on the N—H···N hydrogen bridges between the pyridyl units of the proton sponge H_2tppz^{2+} (Figure 1).[9]

The underlying principle governing ferroelectricity in these supramolecules has also been simplified into a single-component system that can both donate and accept protons.[10,11] A moderate electric field at room temperature was found to switch a very large polarization: croconic acid[10] shows a spontaneous polarization (~21 μC cm^{-2}) as high as that of $BaTiO_3$ (26 μC cm^{-2}). These observations encouraged us to explore electronic functionalities arising from hydrogen-bonded molecular systems.

With the aim of further improving ferroelectric and related properties, we have investigated a variety of supramolecules of H_2xa and 2,3-di(2-pyridinyl)pyrazine (dppz). dppz contains four nitrogen atoms in one pyrazine and two pyridine rings[12] and is structurally related to tppz (Figure 1).[13] The heterocyclic rings of dppz can be flexibly twisted with respect to each other, allowing various intermolecular hydrogen bonds. Two pyridyl nitrogen atoms can also behave as a proton sponge to capture protons from the acid,[14] as observed for tppz salts. Herein, we report above-room-temperature ferroelectricity as well as valence instability and discuss the roles of the supramolecular structures.

2. RESULTS AND DISCUSSION

2.1. Formation of Supramolecules and Polymorphism. The 1:1 cocrystals of [H-dppz][Hca] and [H-dppz][Hba] (α form) were obtained as the main products of diffusing dppz and the corresponding acid in acetone; these black rod crystals exhibited ferroelectricity as described below. We also found additional crystal forms with H_2ba: The diffusion procedure or slow concentration of the 1:1 stoichiometric mixture solution occasionally gave dark brown thin plate crystals of $[H_{1.5}\text{-dppz}]_2[Hba]_3$ (β form) or reddish-brown plate crystals of $[H\text{-dppz}]_2[Hba]_2[H_2ba]$ (γ form). (Note that $H_{1.5}$-dppz$^{1.5+}$ cation signifies a crystallographically averaged form between diprotonated H_2-dppz^{2+} and monoprotonated H-dppz$^+$ species through the two-site disorder of the proton.) These 1:1 and 2:3 stoichiometric forms can be readily discriminated by their crystal appearances under a microscope (Figure 2a).

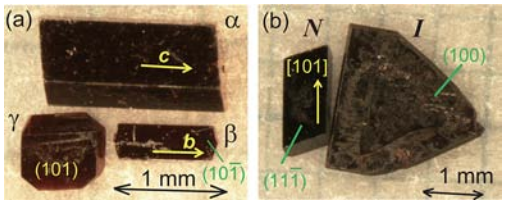

Figure 2. Photographs of cocrystals of dppz. (a) [H-dppz][Hba] (α-form), $[H_{1.5}\text{-dppz}]_2[Hba]_3$ (β-form), and $[H\text{-dppz}]_2[Hba]_2[H_2ba]$ (γ-form) crystals. (b) Neutral [dppz][H_2fa] and ionic [H-dppz][Hfa]·MeOH crystals.

For the fluorine analogue, black rod crystals of 1:1 [dppz][H_2fa] were grown by slow evaporation of ethanol solution containing a stoichiometric mixture of base and acid, whereas methanol was solvated as [H-dppz][Hfa]·MeOH to give brownish plate crystals. These two crystal forms are shown in Figure 2b. It should be noted that the former crystal comprises neutral molecules of dppz and H_2fa, whereas the latter is a proton-transferred salt, as demonstrated in the following experimental results.

2.2. Infrared Absorption Spectra and Ionicity. Removing hydroxyl protons can transform the anilic acid molecule from neutral H_2xa through the Hxa$^-$ monoanion to the xa^{2-} dianion. Because the pK_1 and pK_2 values of H_2xa[15] are similar to the pK_1 value of dppz (2.9−3.1),[16] there can be a change in the degree of proton transfer with a subtle change in the molecular environments of the cocrystals. Infrared spectroscopy is an easy method for judging whether the molecules are neutral or in proton-transferred ionic states; both H_2xa and Hxa$^-$ exhibit a strong absorption band associated with the C═O stretching mode at around 1650 cm^{-1}, but only Hxa$^-$ and xa^{2-} show a band associated with the C—O$^-$ stretching mode at around 1500−1550 cm^{-1}.[7d,17]

The [H-dppz][Hca] cocrystal and three polymorphs from H_2ba exhibit intense C—O$^-$ and C═O stretching-mode bands (Figure 3a). This suggests the presence of a deprotonated species, which is confirmed by the crystal structures discussed in section 2.7. In addition, the distinct crystal structures of the three polymorphs are apparent in the different details in the spectra.

Similar arguments can be applied to the contrasting spectra of [dppz][H_2fa] and its solvated [H-dppz][Hfa]·MeOH form (Figure 3b). The presence or absence of intense bands around 1500−1550 cm^{-1} is related to different degrees of deprotonation of the hydroxyl group; the former is a neutral cocrystal, whereas the latter is a proton-transferred ionic salt. This is consistent with the formula deduced from the X-ray crystallographic studies conducted in this work. The infrared spectra of powdered [dppz][H_2fa] also signal its strong hygroscopic nature (Figure 3c). Compared with the spectrum of the sample carefully dispersed in KBr under dry atmosphere (curve 1 in Figure 3c), strong absorption associated with water at 3330 cm^{-1} appears immediately (curves 2 and 3) after the sample is ground with KBr particles in wet air (~60% humidity). The simultaneous evolution of the C—O$^-$ stretching band indicates humidity-mediated proton transfer that forms Hfa$^-$ anions. The fully wet specimen gave a spectrum similar to that of ionic [H-dppz][Hfa]·MeOH (curve 3). (Note that the [dppz][H_2fa]

dx.doi.org/10.1021/ja400318v | J. Am. Chem. Soc. 2013, 135, 4492−4500

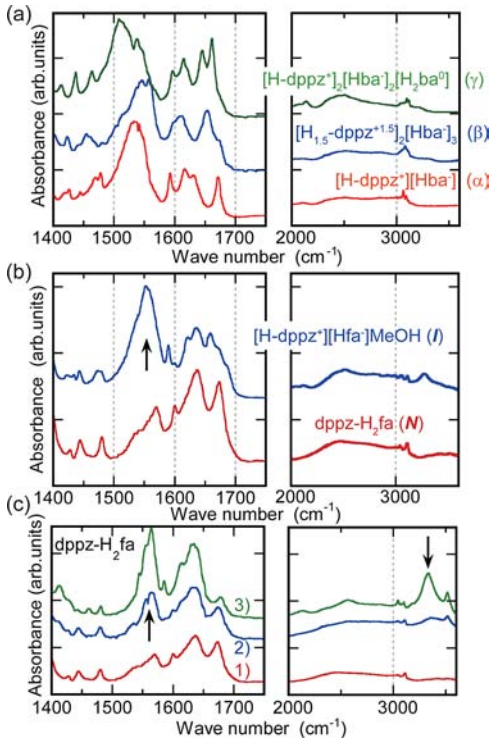

Figure 3. Infrared absorption spectra of powdered cocrystals of dppz and H_2xa (dispersed in a KBr disk). Comparison of the spectra of (a) [H-dppz][Hba] (α-form), $[H_{1.5}\text{-dppz}]_2[Hba]_3$ (β-form), and $[H\text{-dppz}]_2[Hba]_2[H_2ba]$ (γ-form) cocrystals and (b) neutral [dppz][H_2fa] and ionic [H-dppz][Hfa]·MeOH. (c) Hygroscopic nature of neutral [dppz][H_2fa] powder. The KBr disks were prepared by grinding the samples under dry argon (curve 1), quickly in air (curve 2), and finely in air (curve 3). The arrows indicate the absorption bands of water and Hfa^- ions.

single crystal itself is stable in the bulk and retains its lustrous surface in air for a prolonged time.) These observations suggest that [dppz][H_2fa] has a valence instability between the neutral and proton-transferred ionic states. Similar behavior is also observed for the solution spectra, as described in the next section.

2.3. Electronic Spectra of [dppz][H_2fa] in Solution. The dppz and H_2fa mixture was found to behave similarly to a solvatochromic dye. The ethanol solution of [dppz][H_2fa] is brownish yellow, and the methanol solution exhibits a reddish color (Figure 4a). This observation is associated with the bathochromic shift of the optical absorption around 400−600 nm (Figure 5). Because both neutral dppz and its protonated form are transparent in the visible region, these bands arise from H_2fa and/or its deprotonated species. For comparison, the solution spectra of neutral H_2fa (λ_{max} = 432 nm) and ionic Hfa^- in the [H-tmbp][Hfa] salt (λ_{max} = 538 nm, tmbp =4,4′,5,5′-tetramethyl-2,2′-bipyridine[18]) are also shown. In analogy with chloranilic acid,[19] protonated form H_2fa and its conjugate base Hfa^- exhibit distinct absorption spectra (acidichromism[20]). The spectral change arises from the different concentrations of the two species coexisting in solutions of [dppz][H_2fa]. Whereas most of the H_2fa molecules remain in a neutral acidic form in ethanol solution, methanol solution promotes their deprotonation. This equilibrium difference in solution is in good correspondence with the crystallizations of the neutral and ionic solids from the respective solutions.

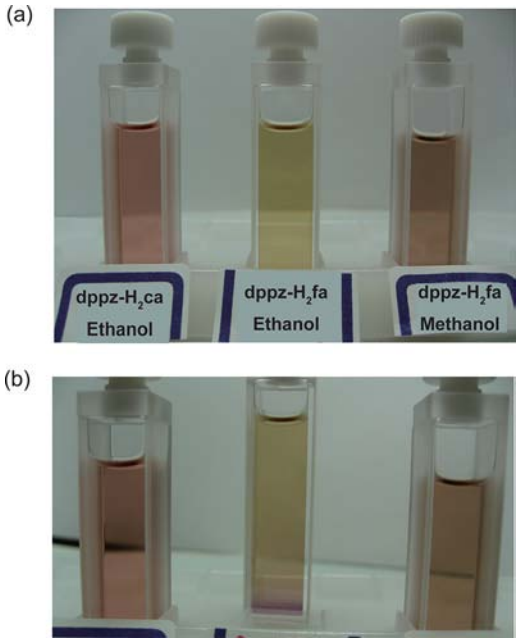

Figure 4. Solvatochromic-like behavior of a 1:1 mixture of dppz and H_2fa. (a) Photographs of the quartz cells containing solutions of [dppz][H_2fa] in ethanol and methanol in comparison with an ethanol solution of [H-dppz][Hca]. (b) Color change after addition of one droplet of methanol to the ethanol solution of [dppz][H_2fa] (central cell).

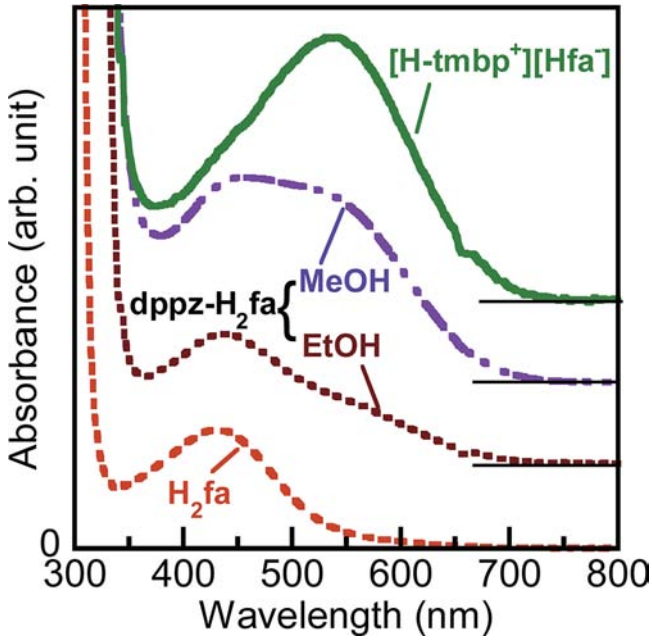

Figure 5. Electronic spectra of ethanol and methanol solutions of [dppz][H_2fa] in comparison with those of ethanol solutions of neutral H_2fa and deprotonated Hfa^- monoanion (dissolved as [H-tmbp][Hfa]).

We also found that addition of a droplet of methanol or water immediately changed the solution of [dppz][H_2fa] in ethanol from a brownish to reddish color, as can be seen around the bottom of the quartz cell in Figure 4b. These observations can be understood in terms of the polarity of the additive solvents; the higher solvent polarities of water and methanol compared to that of ethanol favor the ionic and

dx.doi.org/10.1021/ja400318v | J. Am. Chem. Soc. 2013, 135, 4492−4500

dipolar species and facilitate deprotonation.[21] This phenomenon is also closely related to the humidity-mediated proton transfer observed in the solid state. From these observations, H_2fa and dppz are regarded to be the best-balanced combinations in terms of proton affinity to sufficiently adjust the degree of proton transfer through a subtle change in the environment in both the solution and crystalline states.

2.4. Dielectric Properties. Measurement of relative permittivity is a facile tool for determining the dielectric response from proton dynamics as well as identifying the Curie point of ferroelectricity. Among the cocrystals studied, [H-dppz]$_2$[Hba]$_2$[H_2ba] (γ form) and [H-dppz][Hfa]·MeOH did not display either dipolar fluctuations or phase transitions; the relative permittivity was small (5−6) and independent of temperature between 295 and 5 K, when the electric field was applied normal to the (100) and (101) planes, respectively. Despite the absence of ferroelectricity, [$H_{1.5}$-dppz]$_2$[Hba]$_3$ (β form) revealed a large relative permittivity, the details of which are provided in the Supporting Information. The detailed dielectric properties of the ferroelectric crystal forms are described in the next two sections.

2.4.1. [H-dppz][Hca] and [H-dppz][Hba] (α Form). Figure 6a displays the temperature dependence of the relative permittivity ε_r for [H-dppz][Hca] and the Br-substituted isomorph (α form) measured with the electric field applied along [001], which is parallel to the hydrogen-bonded chains. For [H-dppz][Hca], ε_r, which is as high as 20−30 at room temperature, decreases with increasing ac frequency f and monotonically increases with temperature; at f = 1 kHz, ε_r exceeds 400 at the high-temperature limit of the measurements (T = 380 K). For this reason, the thermal fluctuations of the dipoles and/or polar domains in the cocrystal are expected to become significant as the temperature approaches the Curie point, and a phase transition was in fact detected at 402 K in the calorimetric measurements (see section 2.6). The permittivity of the isomorphous α-[H-dppz][Hba] crystal is independent of temperature up to 380 K, and the inactive dipolar fluctuation implies a much higher Curie point. This behavior is reminiscent of croconic acid, which exhibits a thermally robust ferroelectric phase up to the sample degradation temperature (~450 K). The Curie point of α-[H-dppz][Hba] (if it exists) far exceeds those of other supramolecular ferroelectrics.

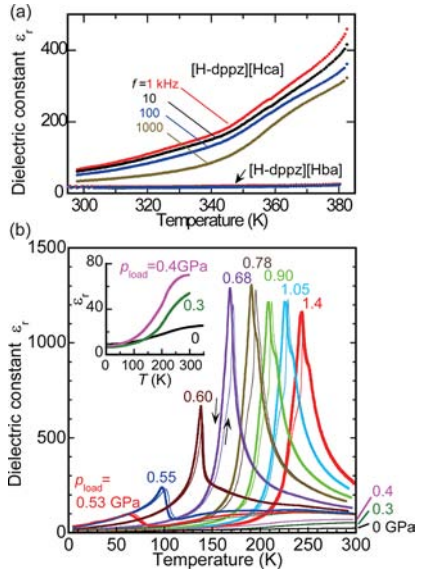

Figure 6. Temperature dependence of the relative permittivity ε_r. (a) [H-dppz][Hca] and [H-dppz][Hba] (α-form) crystals measured with an ac field of various frequencies applied along the hydrogen-bonded chain (parallel to the crystallographic c axis). (b) One [dppz][H_2fa] crystal under various pressures. The ac field (f = 100 kHz) was applied along the crystal [101] direction. The inset shows the data in the low-pressure range.

2.4.2. Neutral [dppz][H_2fa] under Ambient and High Pressures. For the neutral [dppz][H_2fa] crystal, the temperature-dependent permittivity does not signify a Curie point at ambient pressure. Instead, when an electric field (E) is applied along the hydrogen-bonded chains (E ∥ [101]), ε_r gradually increases to 25, implying the presence of some dipolar fluctuation at elevated temperatures up to 350 K (Figure 6b). Very similar behavior was reported for the pressure-induced ferroelectric Phz-H_2fa crystal.[22]

Considering the origins of solvatochromic-like behavior, we anticipated that some external stimuli such as hydrostatic pressure would likely transform neutral [dppz][H_2fa] into dipolar ionic [H-dppz$^+$][Hfa$^-$] accompanied by the emergence of ferroelectricity. As depicted in the inset in Figure 6b, the permittivity increased with pressure in the low-pressure range. With a load of 0.53 GPa, a sharp peak suddenly emerged at 65 K, which is indicative of the expected pressure-induced phase transition. Application of a higher hydrostatic pressure rapidly increased both the height and temperature of the peak anomaly. The ferroelectricity with spontaneous polarization along the hydrogen-bonded chain was manifested in the divergently increasing ε_r value up to 1300. The permittivity peaks were accompanied by a slight thermal hysteresis characteristic of a first-order phase transition.

Figure 7 displays the pressure−temperature phase diagram compiled from the peak temperature and pressure of ε_r, the latter of which was corrected by thermal changes in the contracting pressure-transmitting medium[23] (see Experimental Section). The upward curvature of the phase boundary is very similar to that of the paraelectric−ferroelectric phase boundary of Phz-H_2fa.[22] However, unlike Phz-H_2fa, the [dppz][H_2fa] crystal undergoes a first-order ferroelectric phase transition without passing through any additional lower-temperature phases. In addition, the pressure-induced phases of the two crystals should be different in nature. Phz-H_2xa cocrystals exhibit face-to-face π-molecular stacks that would increase the strength of the repulsive Coulomb interactions upon ionization. Consequently, proton transfer from acid to base is incomplete and related to the appearance of lattice-modulated phases. In

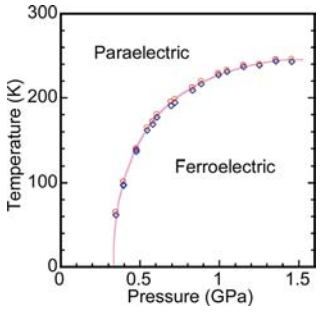

Figure 7. Temperature−pressure phase diagram of [dppz][H_2fa] crystal.

dx.doi.org/10.1021/ja400318v | J. Am. Chem. Soc. 2013, 135, 4492−4500

contrast, the dppz (or H_2fa) molecule is well separated from its neighboring dppz (or H_2fa) molecules, and their diminished repulsion might allow complete proton transfer under high pressure. This conjecture will require future validation from elaborate structural characterizations of the pressurized crystal.

2.5. Ferroelectric Properties. The [H-dppz][Hca] and α-[H-dppz][Hba] crystals revealed ferroelectricity along the hydrogen-bonded chains (i.e., $E \| c$) at room temperature, as evidenced by the parallelogram-shaped hysteresis loops in the electric polarization (P) versus electric field (E) diagrams (Figure 8). At the lowest ac frequency, relatively high remanent

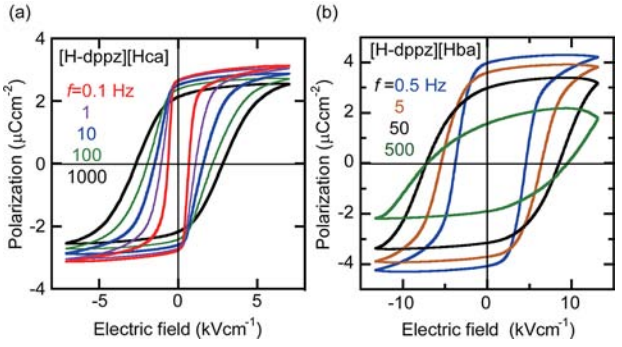

Figure 8. Electric polarization (P)−electric field (E) hysteresis loops of (a) [H-dppz][Hca] and (b) [H-dppz][Hba] (α-form) crystals at room temperature. A triangular ac electric field of various frequencies was applied along the crystal c direction.

polarizations of 2.7 μC cm^{-2} (f = 0.1 Hz) and 4.0 μC cm^{-2} (f = 0.5 Hz) and small coercive fields of 0.7 and 4 kV cm^{-1}, respectively, were observed. As E_c increases with increasing f, the P−E loops are deformed (Figure 8) simply because of the high f exceeding the polarization reversal rate. Specifically, the amplitude of the applied electric field strongly affects the dynamics of the domain walls, that is, the boundaries between the ferroelectric domains of different polarities.

To examine the electric endurance of the high-temperature ferroelectric [H-dppz][Hba], the ferroelectric fatigue properties were investigated by continuously loading a rectangular pulse voltage (f = 100 Hz, amplitude E_p = 10 kV cm^{-1} > E_c) and repeating the P−E hysteresis measurements with a triangular waveform voltage (f = 1 Hz, E_{max}= 13 kV cm^{-1}) and a constant interval on a logarithmic time scale. Figure 9 depicts the change in the remanent polarization, P_r, and coercive field, E_c. Both P_r and E_c increased gradually as the cycle number N increased for $N < 10^4$ (the $N = 10^5$ curve from the initial run is shown in the inset). The electric oscillation possibly releases some domains that were originally pinned around impurities or defects and then develops P_r. Beyond $N = 10^5$ cycles, P_r suddenly started to decrease because the gradually increasing coercive field approached the maximum applied field value. Ferroelectric fatigue with hardening of the polarization reversal might originate from degradation near the interface with the electrodes, for example, impurity injection, charge trapping, and/or diffusion loss of protons. It should be noted that the hysteresis curves shown in Figure 8 are those obtained with nearly maximized polarizations after these electric treatments. The behavior observed here is quite similar to the observations in croconic acid, a hydrogen-bonded ferroelectric.

The P−E curves were also examined at room temperature in $[H_{1.5}$-dppz$]_2$[Hba]$_3$ (β form), which revealed a relatively large permittivity for the $E \| [101]$ and $E \perp (10\bar{1})$ configurations

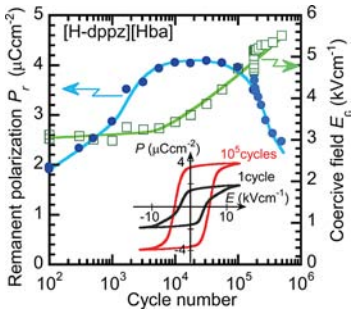

Figure 9. Fatigue behavior of the ferroelectricity in [H-dppz][Hba] crystal at room temperature. Changes in the remanent polarization P_r (solid circles) and coercive field E_c (open squares) as a function of the (total) number of continuously applied voltage pulses (rectangular waveform, f^{pulse} = 100 Hz, E^{pulse}_{max} = 10 kV/cm > E_c). P−E hysteresis measurements with the triangular waveform voltage (f = 1 Hz, E_{max}= 13 kV/cm) were repeated with a constant interval on a logarithmic time scale. Inset: P−E hysteresis loops before and after application of the first 10^5 pulses.

(Figure S1, Supporting Information). We found a simple linear P−E curve, which indicates neither ferroelectricity nor antiferroelectricity, even with an applied maximum field of 100 kV/cm for both crystal directions.

2.6. Thermal Properties. The ferroelectric [H-dppz][Hca] and [H-dppz][Hba] salts decompose at 448−455 and 440−444 K, respectively. Differential scanning calorimetry (DSC) tests indicated that the Curie point might be far above room temperature. The [H-dppz][Hca] salt exhibits a pair of exothermic and endothermic peaks indicative of the phase transition around T = 402 K (Figure S2, Supporting Information), which can be defined as the Curie point, as suggested by the rapid change in the permittivity (Figure 6a). The transition entropy, ΔS, was estimated by integrating the anomalous part of the heat flow and then dividing by the molar amount of sample and transition temperature. For order−disorder phase transitions having g possible configurations, the entropy change is expressed by

$$\Delta S = R \ln g \quad (1)$$

where R = 8.31 J K^{-1} mol^{-1}.

With ΔS = 1.01 J K^{-1} mol^{-1}, we obtained a relatively large g value (1.13) that suggests an order−disorder character mainly in the present phase transition but that is much smaller than 2, which is expected for the disordered hydrogen-bonded protons between the proton donor and acceptor molecules. This would reflect the strong correlations of multiple protons interacting through the π-electron system. By contrast, for [H-dppz][Hba], the absence of corresponding peak anomalies upon heating to 420 K indicates a persistent ferroelectric phase in agreement with the observation of the flat ε−T curves.

2.7. Structural Properties. To understand the microscopic origin of ferroelectricity and the nature of polymorphism and solvatochromic-like behavior, the crystal structures were determined by X-ray diffraction experiments. Table S1 (Supporting Information) summarizes the structural data for the six cocrystals obtained at room temperature.

2.7.1. Molecular Structures and Geometric Change. 2.7.1.1. Acid Molecules (H_2xa/Hxa$^-$/xa^{2-}). The molecular geometry of each acid molecule in the cocrystals is summarized in Table S2 (Supporting Information) with the neutral,[24] dianion,[25] and proton-transferred monovalent state ([H-

dx.doi.org/10.1021/ja400318v | J. Am. Chem. Soc. 2013, 135, 4492−4500

44dmbp][Hca][26] and [H-tmbp][Hfa]; 44dmbp =4,4′-dimethyl-2,2′-bipyridine) shown for reference and comparison. Note that the substitution of halogen atoms in each state barely changes the bond geometries except those involving the substituents. The neutral form was found in [H-dppz]$_2$[Hba]$_2$[H$_2$ba] (γ form) and 1:1 [dppz][H$_2$fa]. In these crystals, the H$_2$xa molecules occupy an inversion center and hence are exactly planar by symmetry. The C—O, C═O, C—C, and C═C bond distances agree closely with those in the neutral H$_2$xa crystals, as shown in Table S2 (Supporting Information), and the molecular geometry adopts the typical *para*-quinoid structure.

The monovalent Hxa$^-$ form is included in all of the cocrystals except [dppz][H$_2$fa]. The cocrystallization has little affect on the C═O and C═C bond lengths, thus preserving the *para*-quinoid molecular form (see bond lengths *f*, *f*′, and *h* in Table S2, Supporting Information). The Hxa$^-$ anions adopt an asymmetric geometry upon deprotonation of either hydroxyl group in the ferroelectric [H-dppz][Hca] and [H-dppz][Hba] (α-form), as well as in the [H-dppz]$_2$[Hba]$_2$[H$_2$ba] (γ-form) crystal. Compared with the neutral form, the bond geometry around the proton-transferred hydroxyl oxygen exhibits a substantially shortened C—O bond and a lengthened C═C bond (see *e*′ and *h*′ in Table S2, Supporting Information), whereas the corresponding bonds are almost unaffected around the hydroxyl oxygen. The [H$_{1.5}$-dppz]$_2$[Hba]$_3$ (β form) contains both asymmetric and symmetric Hba$^-$ anions. The latter anion allocates protons with one-half site occupancy equally to both oxygen sides, and the local π-bond geometry around the oxygen is nearly intermediate between those with and without protons. These observations indicate clearly that the π-bond geometries are closely interrelated with the degree of protonation.

2.7.1.2. Base Molecules. Protonation should also perturb the molecular geometry of dppz. This effect is most obvious in the C═N—C angle, and it has been demonstrated for pyridine molecules that the C═N—C angle (116−117° for neutral nitrogen) widens to 121−123° upon protonation.[27] For dppz molecules, the angle is 116.4° for the neutral form[12b] and 122.6° and 121.7° for the divalent state.[14] For all of the compounds investigated here, the corresponding angles (ϕ) of the neutral O—H···N and ionic N—H$^+$···O$^-$ hydrogen bond are compared in Table S2 (Supporting Information). These different bonding types are distinguished clearly by the value of ϕ with a borderline at 120° for all of the compounds studied.

The dppz molecule can adopt a planar configuration, as seen for its tetraphenylborate (BPh$_4$) salt,[14] when its two copolanar pridyl rings behave as a proton sponge by capturing the proton into a short N—H—N bridge. Apart from this case, the molecule is typically twisted at the C—C bonds between the pyridyl and pyrazyl rings. The dihedral angle between these planar rings is 41.9° in the neutral dppz crystal[14] and ranges from 22° to 57° in the cocrystals with anilic acids. As listed in Table S3 (Supporting Information), protonated H-dppz$^+$ molecules tend to adopt a larger dihedral angle (Ψ') at the protonated pyridyl site than that (Ψ) at the unprotonated pyridyl site. This would be because steric hindrance is enhanced with ring protonation. The difference, $\Delta\Psi$, between Ψ and Ψ' is very small for the ferroelectric cocrystals, especially for [H-dppz][Hca] (3.8°). This molecular geometry is associated with the pseudosymmetry of 2-fold rotation, which would be retained at temperatures above the Curie point. Note that $\Delta\Psi$ is the largest for the ionic [H-dppz][Hfa]·MeOH crystal.

2.7.2. Ferroelectric [H-dppz][Hca] and [H-dppz][Hba] (α Form). The crystal structures of [H-dppz][Hca] and [H-dppz][Hba] (α form) are isomorphous and belong to a monoclinic system with acentric symmetry [space group *Cc* (No. 9), Figure 10a]. Both the H-dppz$^+$ cation and the Hxa$^-$ anion are located in the general positions. Without the hydrogen-bonding protons, the crystal structure seems to gain pseudosymmetries for which the cation and anion have 2-fold rotation and inversion symmetries, respectively. In fact, a least-squares refinement of the parameters reduced *R* to some extent under the corresponding centric space group *C*2/*c*: *R* = 0.066 for 50 parameters on 575 reflections [$I > 2\sigma(I)$ for $2\theta <$ 55°]. That is, the polar proton ordering must be the major cause of symmetry breaking.

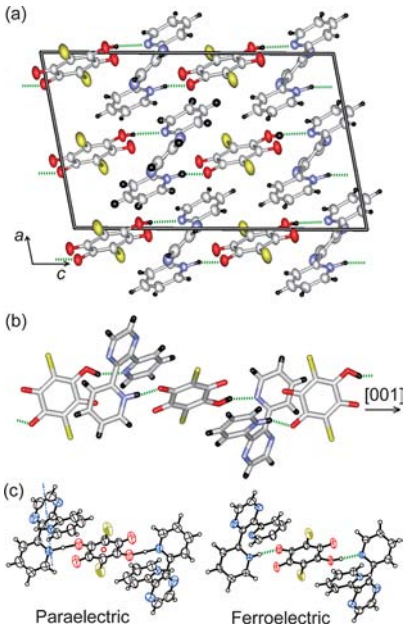

Figure 10. Crystal structures of [H-dppz][Hca] cocrystal. (a) Molecular packing projected along the crystallographic *b* direction. (b) Extended supramolecular chain with intermolecular hydrogen bonds (dotted lines). (c) Structural changes of the hydrogen-bonded supramolecular chain from the paraelectric state (*T* = 410 K, left) to the ferroelectric state (295 K, right). The molecules are viewed along the crystal [1$\bar{1}$0] direction.

In both crystals, each H-dppz$^+$ cation constructs bifurcated hydrogen bonds with the neighboring Hxa$^-$ anion. The unprotonated pyridyl ring forms O—H···N bonds, whereas the protonated ring forms N—H$^+$···O$^-$ bonds with a bifurcated character. At first glance, the molecular packing seems to be rather complicated in crystal structures containing dppz molecules in a twisted conformation. In contrast, the hydrogen-bonded network can be extracted easily as a linear supramolecular chain of acid and base molecules alternating along the crystal [001] direction (Figure 10b).

Importantly, the polarities of the chains are aligned in the same direction (Figure 10a), which generates spontaneous polarization. Furthermore, each chain has a bistable polarity that depends on the locations of the protons (Figure 11). The observed ferroelectricity can thus be explained by cooperative proton transfer in an analogous way to that of the ferroelectric [H-55dmbp][Hia] salt (T_c = 269 K)[8] and the KDP (KH$_2$PO$_4$) family. The stability of the ferroelectric state in the KDP family

dx.doi.org/10.1021/ja400318v | *J. Am. Chem. Soc.* 2013, 135, 4492−4500

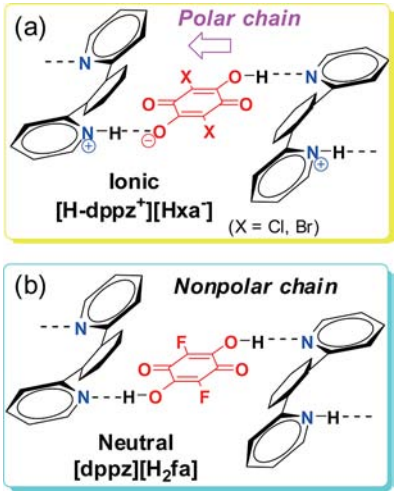

Figure 11. Chemical structures of hydrogen-bonded chains of alternating acid and base molecules.

is governed by the potential barrier height for proton transfer, and the Curie point is well correlated with the hydrogen-bond geometry.[28] The ferroelectric dppz salts actually exhibit much longer distances for both O—H···N and N—H$^+$···O$^-$ bonds ($d_{O\cdots N}^{(1)}$ = 2.75−2.77 Å and $d_{N\cdots O}^{(1)}$ = 2.63 Å for the O···N and N···O distances, respectively; see also Table S3, Supporting Information) than [H-55dmbp][Hia] ($d_{O\cdots N}^{(1)}$ = 2.61−2.70 Å, $d_{N\cdots O}^{(1)}$ = 2.54−2.55 Å) with a lower T_c of 269 K. The Curie point is also elevated with an increase of 0.01−0.02 Å in $d_{O\cdots N}^{(1)}$ and $d_{N\cdots O}^{(1)}$ from [H-dppz][Hca] (T_c = 402 K) to [H-dppz][Hba] (T_c > 420 K). Therefore, some steric hindrance for elongating hydrogen bonds should be a promising approach to thermally robust ferroelectricity for such KDP-like organic crystals.

2.7.3. [H-dppz][Hca] at High Temperature (HT Form). The structural change of [H-dppz][Hca] at the phase transition (T_c = 402 K) was examined by synchrotron X-ray diffraction. We first checked the degree of crystal symmetry breaking in the bulk by probing the intensity difference between the Bijvoet pair (*hkl* versus $\overline{hkl}$) reflections (respective intensities of I_+ and I_-), which arises from the anomalous X-ray scattering effect. If the crystal has centric symmetry or the acentric crystal has equal volume fractions of domains of opposite polarities (i.e., a Flack parameter equal to 0.5), it must obey Friedel's law: I_+/I_- = 1. The [H-dppz][Hca] crystal used in this study exhibited an obvious deviation of I_+/I_- from unity for the Bijvoet pair of $60\bar{4}$ and $\bar{6}04$ at room temperature (Figure S3, Supporting Information). Thus, the crystal must be polar, in agreement with the observation of ferroelectricity. The deviation decreases with temperature and disappears at T_c, indicating a structural change to centric symmetry as expected for the paraelectric state.

At T = 410 K > T_c, the crystal structure was satisfactorily solved with the centric symmetry of the space group $C2/c$ (the minimal supergroup of Cc symmetry). The cation and anion acquire 2-fold rotation and inversion symmetries, respectively, and all of the hydrogen-bonding sites become crystallographically equivalent. A differential Fourier synthesis gave a single maximum in the electron density between the hydrogen-bonded oxygen and nitrogen, as shown by the hydrogen locations in the Figure 10c. This high-temperature structure thus represents the paraelectric form in which the N—H$^+$···O$^-$ and N···H—O bond configurations are thermally averaged by the proton dynamics over single or shallow double potential minima.

2.7.4. β and γ Forms. The crystal structures of both [H-dppz]$_2$[Hba]$_2$[H$_2$ba] (*β* form) and [H$_{1.5}$-dppz]$_2$[Hba]$_3$ (*γ* form) exhibit centric crystal symmetry, in agreement with the absence of ferroelectricity. The full details of molecular arrangements are provided in the Supporting Information.

2.7.5. [dppz][H$_2$fa] (Neutral Form). The crystal structure of [dppz][H$_2$fa] belongs to the monoclinic system with centric symmetry [space group $C2/c$ (No. 15), Figure 12a]. The dppz and H$_2$fa molecules have 2-fold rotation and inversion symmetry, respectively.

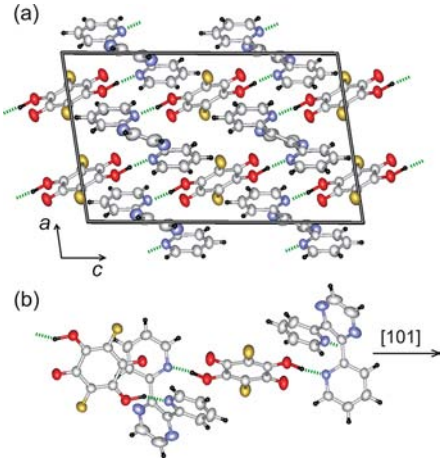

Figure 12. Crystal structures of [dppz][H$_2$fa] cocrystal. (a) Molecular packing projected along the crystallographic *b* direction. (b) Extended supramolecular chain with intermolecular hydrogen bonds (dotted lines).

Along the [101] direction, the acid and base molecules alternate in a linear chain with intermolecular O—H···N bonds (O···N distances of 2.636 Å). The overall molecular arrangement in each chain is very similar to those in the ferroelectric [H-dppz][Hca] and [H-dppz][Hba] (*α*-form) crystals (compare Figures 10a and 12a). The only difference is that the neutral chains in the former compound are nonpolar and the ionic chains in the latter are dipolar and ferroelectric (Figure 11). Therefore, the dipolar fluctuation observed in the permittivity along the supramolecular chain of [dppz][H$_2$fa] is likely to be related to the response from thermally excited dipolar ionic domains (or strings), considering the neutral−ionic instability in both the solution and solid forms.

2.7.6. [H-dppz][Hfa]·MeOH (Ionic Form). The crystal structure of [H-dppz][Hfa]·MeOH belongs to the monoclinic system (Figure 13a). All of the molecules are located in general positions. The space group is acentric Cc (No. 9), identical to that of the ferroelectric [H-dppz][Hca] crystal. However, the structure of the Hfa salt does not show any additional pseudosymmetry even without protons and is therefore not ferroelectric but simply dipolar. An infinite supramolecular chain is constructed along the crystal *b* direction from alternating Hfa$^-$ anions and methanol molecules with hydrogen bonds of very short O—H···O$_{MeOH}$ (2.584 Å) and O$^-$···H—O$_{MeOH}$ (2.723 Å) distances (Figure 13b). The protonated pyridyl ring of the H-dppz$^+$ cation forms a N—H$^+$···O$^-$ bond with the deprotonated oxygen of the Hfa$^-$ anion. The unprotonated pyridine and pyrazine rings, however, are not

dx.doi.org/10.1021/ja400318v | J. Am. Chem. Soc. 2013, 135, 4492−4500

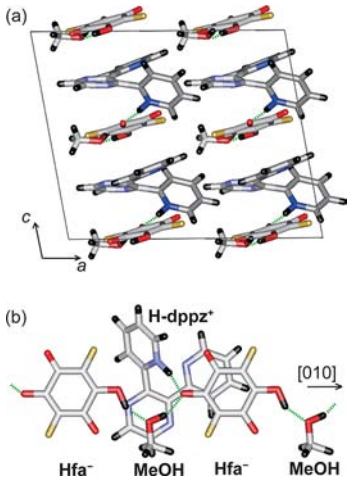

Figure 13. Crystal structures of [H-dppz][Hfa]·MeOH cocrystal. (a) Molecular packing projected along the crystallographic *b* direction. (b) Extended supramolecular chain of alternating Hfa^- and MeOH molecules with a H-$dppz^+$ cation attached as a pendant.

involved in the hydrogen bonds. Thus, the H-$dppz^+$ cation appears as a pendant simply bonded to the linear supramolecular chain.

3. CONCLUSIONS

The dppz molecule has proven to be an excellent building block for a variety of supramolecular structures with various twist conformations. Its combination with anilic acid is delicately balanced in terms of the p*K* value, and cocrystallization was found to regulate the degree of proton transfer from the neutral to ionic crystalline forms depending on the acidity. We found room-temperature ferroelectricity in the 1:1 proton-transferred salts of [H-dppz][Hca] and [H-dppz][Hba]. Through the twisted conformation of dppz, these salts construct rather simple linear supramolecular chains of alternating acid and base molecules, which are bistable in polarity. Compared with other supramolecular ferroelectrics, the robust nature of the ferroelectricity to high temperatures of 400 K or more can be attributed to protons in the elongated hydrogen bonds favoring the ordered state.

The combination of fluoranilic acid (H_2fa) and dppz was found to be the best balanced in terms of proton affinity to sufficiently adjust the degree of proton transfer to dppz in both solution and crystalline states. The equilibrium between the neutral and proton-transferred ionic species depends on the solvent polarity, and the consequent spectral changes with different alcohols also affect the crystallization with or without proton transfer: [dppz][H_2fa] and [H-$dppz^+$][Hfa^-]·MeOH. The linear-chain supramolecular structure of paraelectric [dppz][H_2fa] is very similar to that of ferroelectric [H-dppz][Hca], except for the degree of proton transfer. The ferroelectricity induced with a modest hydrostatic pressure corroborates the conclusion that the ionic state with a dipolar [H-$dppz^+$][Hfa^-] chain is energetically close to the nonpolar neutral ground state of the [dppz][H_2fa] crystal.

4. EXPERIMENTAL SECTION

4.1. Materials. Fluoranilic acid was prepared from *p*-fluoranil according to the literature method[15] and purified twice by temperature-gradient sublimation under vacuum. The purity was confirmed by elementary analysis and mass spectra. Commercially available H_2ca, H_2ba, dppz, and 44dmbp were purified by repetitive recrystallization from ethanol or methanol and then twice by gradient sublimation under vacuum. The base tmbp was synthesized according to the literature method[18] and also purified by gradient sublimation under vacuum.

Diffusion of dppz and H_2ca (or H_2ba) in acetone solution gave black rod crystals of ferroelectric [H-dppz][Hca] (or the α form of [H-dppz][Hba]), which decomposes at 175−182 °C (or 167−171 °C). Two additional nonferroelectric crystal forms were also found for H_2ba. Slow evaporation of an ethanol solution of a 1:1 stoichiometric mixture under a stream of argon gas gave dark brown thin-plate crystals of $[H_{1.5}\text{-dppz}]_2[Hba]_3$ (β form). This crystal form was also obtained as a minor product of the diffusion procedure. Upon similar slow evaporation of methanol or ethanol solution, we also found reddish-brown plate crystals of $[H\text{-dppz}]_2[Hba]_2[H_2ba]$ (γ form). Black rod crystals of [dppz][H_2fa] were obtained by slow evaporation of an ethanol solution containing a stoichiometric mixture of base and acid. With the use of methanol, we obtained brownish plate crystals of the solvated form [H-dppz][Hfa]·MeOH.

[H-44dmbp][Hca] and [H-tmbp][Hfa] cocrystals were prepared to identify the typical optical spectra and molecular geometry of the monovalent Hca^- and Hfa^- anions. The former salt was obtained as a single crystal by the slow evaporation of its methanol solution and the latter by diffusing tmbp and H_2fa in ethanol solution.

4.2. Spectroscopy and Calorimetry. Infrared absorption spectra of the samples dispersed in a KBr disk were recorded at room temperature with a JASCO FTIR-200 spectrometer over a wavelength range of 4000−400 cm^{-1} at a resolution of 4 cm^{-1}. Electronic absorption spectra in solution were measured with a Hitachi U-3500 UV−vis spectrometer. The melting or decomposition points were checked on a Yanako MP-500D apparatus prior to differential scanning calorimetry. The thermal analysis was performed using a Seiko Instruments DSC220C differential scanning calorimeter. The sample was encapsulated in an aluminum pan and heated at a rate of 5 K min^{-1}. The temperature was calibrated using the melting point of indium (429.8 K). Synthetic sapphire was used as the standard for the determination of the heat capacity.

4.3. Electric Measurements. All electric measurements were obtained from as-grown single crystals with painted gold or silver electrodes. The dielectric constant was measured with an LCR meter (HP 4284A). Hydrostatic pressure was generated in a clamp-type high-pressure cell using a pressure-transmitting oil (Idemitsu Kosan Daphne 7373). The applied pressure at each transition point was obtained by correcting the thermal change of pressure with 7.6×10^{-4} GPa K^{-1} (for $T > 90$ K) due to contraction of the medium.[23] The cooling and heating rates were 1−2 K min^{-1}, and the accuracy in the temperature was ∼0.05 K.

The electric polarization (*P*)−electric field (*E*) hysteresis curves were collected on a ferroelectrics evaluation system (Toyo Corporation, FCE-1) consisting of a current/charge−voltage converter (Toyo Corporation, model 6252), an arbitrary waveform generator (Biomation 2414B), an analog-to-digital converter (WaveBook 516), and a voltage amplifier (NF Corporation, HVA4321). The measurements were performed at room temperature with a high-voltage triangular wave field and various alternating frequencies. The ferroelectric hysteresis loops were successfully obtained in air for both [H-dppz][Hca] and [H-dppz][Hba] crystals having a modest coercive field. The $[H_{1.5}\text{-dppz}]_2[Hba]_3$ (β-form) crystal, for which no dielectric hysteresis loops were identified, was examined by immersing the crystal in silicon oil to prevent atmospheric discharge under a high electric field (80−100 kV cm^{-1}).

4.4. Crystallographic Studies. The crystallographic data and experimental details for the cocrystals of dppz are summarized in Table S1 (Supporting Information). Both the X-ray diffraction data collection at room temperature and the assignment of the crystallographic axes of the bulk single crystals were completed using a Rigaku AFC7R four-circle diffractometer equipped with a Mercury CCD area detector (graphite-monochromated Mo Kα radiation).

The temperature-dependent structural changes were also examined for the ferroelectric [H-dppz][Hca] crystal. Data were collected at

dx.doi.org/10.1021/ja400318v | *J. Am. Chem. Soc.* 2013, 135, 4492−4500

various temperatures above room temperature with a Rigaku DSC imaging plate system using Si double-crystal monochromatized synchrotron radiation (λ = 0.6876 Å) at the BL-8A beamline of the Photon Factory (PF), High-Energy Accelerator Research Organization (KEK). The monochromatized beam was focused using a bent cylindrical mirror made of a Si crystal coated with Rh to produce a focused beam size of 0.3 mm (vertical) × 0.7 mm (horizontal). The crystal attached to a glass fiber was heated by flowing nitrogen gas. The full data collection for the structural analysis was obtained at 295 and 410 K to compare the structural changes before and after the phase transition at T_c = 402 K.

The Rapid-AUTO program from Rigaku Corporation was employed for the two-dimensional image processing of the synchrotron X-ray data. The CrystalStructure crystallographic software packages from Molecular Structure Corporation (MSC) and Rigaku Corporation were employed for the direct method and refinement of the structures. The final refinements of the non-hydrogen atoms were performed with anisotropic thermal factors.

The data were deposited at Cambridge Crystallographic Data Center as supplementary publications CCDC-925615−925624.

■ ASSOCIATED CONTENT

Ⓢ Supporting Information

Detailed characterization (dielectric properties and crystal structures) for the nonferroelectric polymorphs, calorimetric data (DSC) for [H-dppz][Hca], crystallographic details for all of the dppz cocrystals along with CIF files. This material is available free of charge via the Internet at http://pubs.acs.org.

■ AUTHOR INFORMATION

Corresponding Author

s-horiuchi@aist.go.jp

Notes

The authors declare no competing financial interest.

■ ACKNOWLEDGMENTS

This work was partially supported by KAKENHI (No. 20110003 from MEXT, No. 23340111 from JSPS) and by the Japan Society for the Promotion of Science (JSPS) through "Funding Program for World-Leading Innovative R&D on Science and Technology (FIRST Program)" initiated by the Council for Science and Technology Policy (CSTP). The synchrotron X-ray study was performed with the approval of the Photon Factory Program Advisory Committee (No. 2009S2-003).

■ REFERENCES

(1) Jeffery, G. A. *An Introduction to Hydrogen Bonding*; Oxford University Press: Oxford, U.K., 1997.

(2) (a) Lines, M. E.; Glass, A. M. *Principles and Applications of Ferroelectrics and Related Materials*; Oxford University Press: New York, 1977. (b) Uchino, K. *Ferroelectric Devices*; Marcel Dekker: New York, 2000. (c) Dawber, M.; Rabe, K. M.; Scott, J. F. *Rev. Mod. Phys.* **2005**, *77*, 1083−1130.

(3) Busch, G.; Scherrer, P. *Naturwissenschaften* **1935**, *23*, 737−738.

(4) (a) Ling, Q.-D.; Liaw, D.-J.; Zhu, C.; Chan, D. S.; Kang, E.-T.; Neoh, K.-G. *Prog. Polym. Sci.* **2008**, *33*, 917−978. (b) Heremans, P.; Gelinck, G. H.; Müller, R.; Baeg, K.-J.; Kim, D.-Y.; Noh, Y.-Y. *Chem. Mater.* **2011**, *23*, 341−358. (c) Naber, R. C. G.; Asadi, K.; Blom, P. W. M.; de Leeuw, D. M.; de Boer, B. *Adv. Mater.* **2010**, *22*, 933−945. (d) Asadi, K.; Li, M.; Blom, P. W. M.; Kemerink, M.; de Leeuw, D. M. *Mater. Today* **2011**, *14*, 592−599.

(5) (a) Fousek, J. *Ferroelectrics* **1991**, *113*, 3−20. (b) Sworakowski, J. *Ferroelectrics* **1992**, *128*, 295−306. (c) Horiuchi, S.; Tokura, Y. *Nat. Mater.* **2008**, *7*, 357−366.

(6) Kitagawa, S.; Kawata, S. *Coord. Chem. Rev.* **2002**, *224*, 11−34.

(7) (a) Horiuchi, S.; Ishii, F.; Kumai, R.; Okimoto, Y.; Tachibana, H.; Nagaosa, N.; Tokura, Y. *Nat. Mater.* **2005**, *4*, 163−166; **2008**, *7*, 922 (corrigendum).. (b) Horiuchi, S.; Kumai, R.; Tokura, Y. *J. Am. Chem. Soc.* **2005**, *127*, 5010−5011. (c) Kumai, R.; Horiuchi, S.; Sagayama, H.; Arima, T.; Watanabe, M.; Noda, Y.; Tokura, Y. *J. Am. Chem. Soc.* **2007**, *129*, 12920−12921. (d) Horiuchi, S.; Kumai, R.; Tokura, Y. *J. Mater. Chem.* **2009**, *19*, 4421−4434.

(8) Horiuchi, S.; Kumai, R.; Tokura, Y. *Angew. Chem., Int. Ed.* **2007**, *46*, 3497−3501.

(9) Horiuchi, S.; Kumai, R.; Tokunaga, Y.; Tokura, Y. *J. Am. Chem. Soc.* **2008**, *130*, 13382−13391.

(10) Horiuchi, S.; Tokunaga, Y.; Giovannetti, G.; Picozzi, S.; Itoh, H.; Shimano, R.; Kumai, R.; Tokura, Y. *Nature* **2010**, *463*, 789−792.

(11) (a) Horiuchi, S.; Kumai, R.; Tokura, Y. *Adv. Mater.* **2011**, *23*, 2098−2103. (b) Horiuchi, S.; Kagawa, F.; Hatahara, K.; Kobayashi, K.; Kumai, R.; Murakami, Y.; Tokura, Y. *Nat. Commun.* **2012**, *3*, 1308.

(12) (a) Goodwin, H. A.; Lions, F. *J. Am. Chem. Soc.* **1959**, *81*, 6415−6422. (b) Huang, N.; Pennington, W. T.; Petersen, J. D. *Acta Crystallogr. C* **1991**, *47*, 2011−2012.

(13) (a) Greaves, B.; Stoeckli-Evans, H. *Acta Crystallogr. C* **1992**, *48*, 2269−2271. (b) Padgett, C. W.; Walsh, R. D.; Drake, G. W.; Hanks, T. W.; Pennington, W. T. *Cryst. Growth Des.* **2005**, *5*, 745−753. (c) Graf, M.; Stoeckli-Evans, H. *Acta Crystallogr. C* **1996**, *52*, 3073−3075.

(14) Robertson, K. N.; Bakshi, P. K.; Lantos, S. D.; Cameron, T. S.; Knop, O. *Can. J. Chem.* **1998**, *76*, 583−611.

(15) Wallenfels, K.; Friedrich, K. *Chem. Ber.* **1960**, *93*, 3070−3082.

(16) Goethals, M.; Zeegers-Huyskens, T. *Spectrosc. Lett.* **1998**, *31*, 737−746.

(17) (a) Fujioka, J.; Horiuchi, S.; Kida, N.; Shimano, R.; Tokura, Y. *Phys. Rev. B* **2009**, *80*, 125134. (b) Fujioka, J.; Horiuchi, S.; Kagawa, F.; Tokura, Y. *Phys. Rev. Lett.* **2009**, *102*, 197601.

(18) Patterson, B. T.; Keene, F. R. *Inorg. Chem.* **1998**, *37*, 645−650.

(19) Kumai, R.; Horiuchi, S.; Okimoto, Y.; Tokura, Y. *J. Chem. Phys.* **2006**, *125*, 084715.

(20) Bouas-Laurent, H.; Dürr, H. *Pure Appl. Chem.* **2001**, *73*, 639−665.

(21) Reichardt, C. *Chem. Rev.* **1994**, *94*, 2319−2358.

(22) Kumai, R.; Horiuchi, S.; Fujioka, J.; Tokura, Y. *J. Am. Chem. Soc.* **2012**, *134*, 1036−1046.

(23) Murata, K.; Yoshino, H.; Yadav, H. O.; Honda, Y.; Shirakawa, N. *Rev. Sci. Instrum.* **1997**, *68*, 2490−2493.

(24) (a) Andersen, E. K.; Andersen, I. G. K. *Acta Crystallogr. B* **1975**, *31*, 384−387. (b) Andersen, E. K. *Acta Crystallogr.* **1967**, *22*, 188−191. (c) Robl, C. *Z. Kristallogr.* **1987**, *180*, 249−253. (d) Robl, C.; Sheldrick, G. M. *Z. Kristallogr.* **1988**, *184*, 295−300.

(25) Andersen, E. K. *Acta Crystallogr.* **1967**, *2*, 196−201.

(26) Bator, G.; Sawka-Dobrowolska, W.; Sobczyk, L.; Grech, E.; Nowicka-Scheibe, J.; Pawlukojć, A.; Wuttke, J.; Baran, J.; Owczarek, M. *J. Chem. Phys.* **2011**, *135*, 044509.

(27) Majerz, I.; Koll, A. *Acta Crystallogr. B* **2004**, *60*, 406−415.

(28) (a) Blinc, R. *J. Phys. Chem. Solids* **1960**, *13*, 204−211. (b) Matsushita, E.; Matsubara, T. *Prog. Theor. Phys.* **1982**, *67*, 1−19. (c) Ichikawa, M.; Motida, K.; Yamada, N. *Phys. Rev. B* **1987**, *36*, 874−876. (d) McMahon, M. I.; Nelmes, R. J.; Kuhs, W. F.; Dorwarth, R.; Piltz, R. O.; Tun, Z. *Nature* **1990**, *348*, 317−319. (e) Bussmann-Holder, A.; Michel, K. H. *Phys. Rev. Lett.* **1998**, *80*, 2173−2176. (f) Koval, S.; Kohanoff, J.; Migoni, R. L.; Tosatti, E. *Phys. Rev. Lett.* **2002**, *89*, 187602.